Chapter 9
Nonlinear Quantum Dissipative Systems

Abstract In the preceding chapter we derived linearised solutions to the quantum fluctuations occurring in some nonlinear systems in optical cavities. In these solutions the quantum noise has been treated as a small perturbation to the solutions of the corresponding nonlinear classical problem. It is not possible, in general, to find exact solutions to the nonlinear quantum equations which arise in nonlinear optical interactions. It has, however, been possible to find solutions to some specific systems. These solutions provide a test of the region of validity of the linearised solutions especially in the region of an instability. Furthermore they allow us to consider the situation where the quantum noise is large and may no longer be treated as a perturbation. In this case, manifestly quantum mechanical states may be produced in a nonlinear dissipative system.

We shall give solutions to the nonlinear quantum equations for two of the problems considered in Chap. 8, namely, the parametric oscillator and dispersive optical bistability.

9.1 Optical Parametric Oscillator: Complex *P* Function

We shall first solve for the steady state of the parametric oscillator using the complex *P* function. Then, we show, using the positive *P* function, that the steady state subharmonic field is in a superposition state. We go on to calculate the tunnelling time between the two states in the superposition.

We consider the degenerate parametric oscillator described in Chap. 8, following the treatment of *Drummond* et al. [1]. The Hamiltonian is

$$\mathscr{H} = \sum_{i=0}^{3} \mathscr{H}_i \tag{9.1}$$

where

$$\mathscr{H}_0 = \hbar\omega a_1^\dagger a_1 + 2\hbar\omega a_2^\dagger a_2 \,, \tag{9.2}$$

$$\mathscr{H}_1 = i\hbar\frac{\kappa}{2}(a_1^{\dagger 2}a_2 - a_1^2 a_2^\dagger)\,, \tag{9.3}$$

$$\mathscr{H}_2 = i\hbar(\varepsilon_2 a_2^\dagger \mathrm{e}^{-2\mathrm{i}\omega t} - \varepsilon_2^* a_2 \mathrm{e}^{2\mathrm{i}\omega t})\,, \tag{9.4}$$

$$\mathscr{H}_3 = a_1\Gamma_1^\dagger + a_2\Gamma_2^\dagger + \mathrm{h.c}\,. \tag{9.5}$$

where a_1 and a_2 are the boson operators for two cavity modes of frequency ω and 2ω, respectively. κ is the coupling constant for the nonlinear coupling between the modes. The cavity is driven externally by a coherent driving field with frequency 2ω and amplitude ε_2. Γ_1, Γ_2 are the bath operators describing the cavity damping of the two modes.

We recall from Chap. 8 that there are two stable steady state solutions depending on whether the driving field amplitude is above or below the threshold amplitude $\varepsilon_2^{\mathrm{c}} = \gamma_1\gamma_2/\kappa$. In particular, the steady states for the low frequency mode α_1 are

$$\begin{aligned}
&\alpha_1^0 = 0, \qquad \varepsilon_2 < \varepsilon_2^{\mathrm{c}}\,,\\
&\alpha_1^0 = \pm\left[\frac{2}{\kappa}(\varepsilon_2 - \varepsilon_2^{\mathrm{c}})\right]^{1/2}, \quad \varepsilon_2 \geq \varepsilon_2^{\mathrm{c}}\,.
\end{aligned} \tag{9.6}$$

The master equation for the density operator of the two modes is

$$\begin{aligned}
\frac{\partial}{\partial t}\rho =& \frac{1}{i\hbar}[\mathscr{H}_0 + \mathscr{H}_1 + \mathscr{H}_2, \rho] + \gamma_1(2a_1\rho a_1^\dagger - a_1^\dagger a_1\rho - \rho a_1^\dagger a_1)\\
&+ \gamma_2(2a_2\rho a_2^\dagger - a_2^\dagger a_2\rho - \rho a_2^\dagger a_2)
\end{aligned} \tag{9.7}$$

where the irreversible part of the master equation follows from (6.44) for a zero-temperature bath. γ_1, γ_2 are the cavity damping rates.

This equation may be converted to a c-number Fokker–Planck equation using the generalized P representation discussed in Chap. 6. Using the operator-algebra rules described in Chap. 6, we arrive at the Fokker–Planck equation

$$\begin{aligned}
\frac{\partial}{\partial t}P(\alpha) = \Bigg\{ &\frac{\partial}{\partial\alpha_1}(\gamma_1\alpha_1 - \kappa\beta_1\alpha_2) + \frac{\partial}{\partial\beta_1}(\gamma_1\beta_1 - \kappa\alpha_1\beta_2)\\
&+ \frac{\partial}{\partial\alpha_2}\left(\gamma_2\alpha_2 - \varepsilon_2 + \frac{\kappa}{2}\alpha_1^2\right) + \frac{\partial}{\partial\beta_2}\left(\gamma_2\beta_2 - \varepsilon_2^* + \frac{\kappa}{2}\beta_1^2\right)\\
&+ \frac{1}{2}\left[\frac{\partial^2}{\partial\alpha_1^2}(\kappa\alpha_2) + \frac{\partial^2}{\partial\beta_1^2}(\kappa\beta_2)\right]\Bigg\} P(\alpha)
\end{aligned} \tag{9.8}$$

where $(\alpha) = [\alpha_1, \beta_1, \alpha_2, \beta_2]$.

An attempt to find the steady state solution of this equation by means of a potential solution fails since the potential conditions (6.73) are not satisfied.

We proceed by adiabatically eliminating the high-frequency mode. This may be accomplished best in the Langevin equations equivalent to (9.8).

$$\frac{\partial}{\partial t}\begin{pmatrix}\alpha_1\\ \beta_1\end{pmatrix}=\begin{pmatrix}\kappa\beta_1\alpha_2-\gamma_1\alpha_1+\sqrt{\kappa\alpha_2}[\eta_1(t)]\\ \kappa\alpha_1\beta_2-\gamma_1\beta_1+\sqrt{\kappa\beta_2}[\tilde{\eta}_1(t)]\end{pmatrix}$$
$$\frac{\partial}{\partial t}\begin{pmatrix}\alpha_2\\ \beta_2\end{pmatrix}=\begin{pmatrix}\varepsilon_2-\frac{\kappa}{2}\alpha_1^2-\gamma_2\alpha_2\\ \varepsilon_2^*-\frac{\kappa}{2}\beta_2^2-\gamma_2\beta_2\end{pmatrix} \tag{9.9}$$

where $\eta_1(t),\ \tilde{\eta}_1(t)$ are delta correlated stochastic forces with zero mean

$$\langle\eta_1(t)\rangle=\langle\tilde{\eta}_1(t)\rangle=\langle\eta_1(t)\eta_1(t')\rangle=\langle\tilde{\eta}_1(t)\tilde{\eta}_1(t')\rangle=0\,, \tag{9.10}$$
$$\langle\eta_1(t)\tilde{\eta}_1(t)\rangle=\delta(t-t')\,. \tag{9.11}$$

Under the conditions $\gamma_2\gg\gamma_1$ we can adiabatically eliminate α_2 and β_2 which gives the resultant Langevin equation for α_1 and β_1

$$\frac{\partial}{\partial t}\begin{pmatrix}\alpha_1\\ \beta_1\end{pmatrix}=\begin{pmatrix}\frac{\kappa}{\gamma_2}\left(\varepsilon_2-\frac{\kappa}{2}\alpha_1^2\right)\beta_1-\gamma_1\alpha_1\\ \frac{\kappa}{\gamma_2}\left(\varepsilon_2^*-\frac{\kappa}{2}\beta_1^2\right)\alpha_1-\gamma_1\beta_1\end{pmatrix}+\begin{pmatrix}\left[\frac{\kappa}{\gamma_2}\left(\varepsilon_2-\frac{\kappa}{2}\alpha_1^2\right)\right]^{1/2} & \eta_1(t)\\ \left[\frac{\kappa}{\gamma_2}\left(\varepsilon_2^*-\frac{\kappa}{2}\beta_1^2\right)\right]^{1/2} & \tilde{\eta}_1(t)\end{pmatrix}\,. \tag{9.12}$$

The Fokker–Planck equation corresponding to these equations is

$$\begin{aligned}\frac{\partial}{\partial t}P(\alpha_1,\beta_1)=&\left\{\frac{\partial}{\partial\alpha_1}\left[\gamma_1\alpha_1-\frac{\kappa}{\gamma_2}\left(\varepsilon_2-\frac{\kappa}{2}\alpha_1^2\right)\beta_1\right]\right.\\&+\frac{\partial}{\partial\beta_1}\left[\gamma_1\beta_1-\frac{\kappa}{\gamma_2}\left(\varepsilon_2^*-\frac{\kappa}{2}\beta_1^2\right)\alpha_1\right]\\&\left.+\frac{1}{2}\left[\frac{\partial^2}{\partial\alpha_1^2}\frac{\kappa}{\gamma_2}\left(\varepsilon_2-\frac{\kappa}{2}\alpha_1^2\right)+\frac{\partial}{\partial\beta_1^2}\frac{\kappa}{\gamma_2}\left(\varepsilon_2^*-\frac{\kappa}{2}\beta_1^2\right)\right]\right\}P(\alpha_1\beta_1)\,.\end{aligned} \tag{9.13}$$

We set $\frac{\partial}{\partial t}P(\alpha_1,\ \beta_1)=0$ and attempt to find a potential solution as given by (6.72). It is found as

$$F_1=-2\left(\beta_1-\frac{2\gamma_2\left(\gamma_1-\frac{\kappa^2}{2\gamma_2}\right)\alpha_1}{2\kappa\varepsilon_2-\kappa^2\alpha_1^2}\right) \tag{9.14}$$

$$F_2=-2\left(\alpha_1-\frac{2\gamma_2\left(\gamma_1-\frac{\kappa^2}{2\gamma_2}\right)\beta_1}{2\kappa\varepsilon_2^*-\kappa^2\beta_1^2}\right) \tag{9.15}$$

It follows that the potential conditions

$$\frac{\partial F_1}{\partial\alpha_1}=\frac{\partial F_2}{\partial\beta_1} \tag{9.16}$$

are satisfied.

The potential is obtained on integrating (9.14 and 9.15)

$$P(\alpha) = N \exp\left[2\alpha_1\beta_1 + \frac{2\bar{\gamma}_1\gamma_2}{\kappa^2}\ln(c^2 - \kappa^2\alpha_1^2) + 2\left(\frac{\bar{\gamma}_1\gamma_2}{\kappa^2}\right)^* \ln(c^{*2} - \kappa^2\beta_1^2)\right] \tag{9.17}$$

where

$$c = \sqrt{2\kappa\varepsilon_2}\,, \qquad \bar{\gamma}_1 = \gamma_1 - \frac{\kappa^2}{2\gamma_2}\,.$$

It is clear that this function diverges for the usual integration domain of the complex plane with $\beta_1 = \alpha_1^*$. The observable moments may, however, be obtained by use of the complex P representation. The calculations are described in Appendix 9.A.

The semi-classical solution for the intensity exhibits a threshold behaviour at $\varepsilon_2 = \varepsilon_2^c = \gamma_1\gamma_2/\kappa$. This is compared in Fig. 9.1 with the mean intensity $I = \langle\beta_1\alpha_1\rangle$ calculated from the solution (9.17), as shown in the Appendix 9.A. For comparison, the mean intensity when thermal fluctuations are dominant (Exercise 9.4) is also plotted. The mean intensity with thermal fluctuations displays the rounding of the transition familiar from classical fluctuation theory. The quantum calculation shows a feature never observed in a classical system where the mean intensity actually drops below the semi-classical intensity. This deviation from the semi-classical behaviour is most significant for small threshold photon numbers. As the parameter $\gamma_1\gamma_2/\kappa^2$ is increased the quantum mean approaches the semi-classical value.

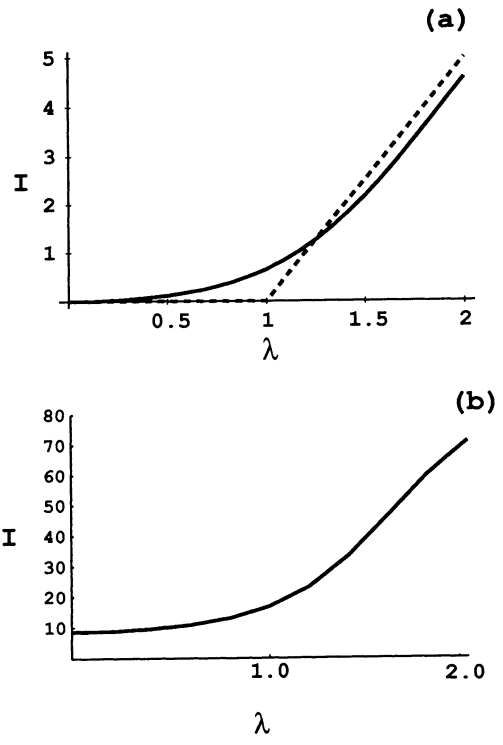

Fig. 9.1 A plot of the mean intensity for the degenerate parametric oscillator versus the scaled driving field λ. (**a**) The case of zero thermal fluctuations. The *dashed curve* represents the semi-classical intensity, the *solid curve* is the exact quantum result. In both cases $\mu^2 = 2\varepsilon_2^c/\kappa = 5.0$. Note that above threshold the exact quantum result is less than the semi-classical prediction. (**b**) The case of dominant thermal fluctuations. The mean thermal photon number is 10.0 and $\mu^2 = 2\varepsilon_2^c/\kappa = 100.0$

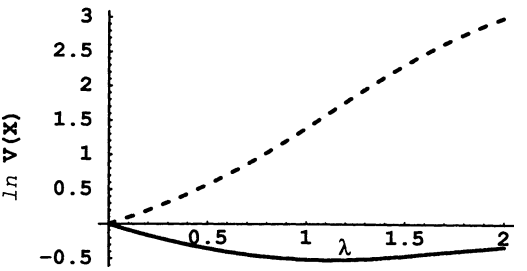

Fig. 9.2 The log variance of the squeezed (*solid*) and unsqueezed (*dashed*) quadrature in a degenerate parametric amplifier versus the scaled driving field with $\mu^2 = 2\varepsilon_2^c/\kappa = 5.0$

The variance of fluctuations in the quadratures $X_1 = a_1 + a_1^\dagger$ and $X_2 = (a_1 - a_1^\dagger)/\mathrm{i}$ is given by

$$\Delta X_1^2 = [\langle(\alpha_1 + \beta_1)^2\rangle - (\langle\alpha_1 + \beta_1\rangle)^2] + 1\,, \tag{9.18}$$

$$\Delta X_2^2 = -[\langle(\alpha_1 - \beta_1)^2\rangle - (\langle\alpha_1 - \beta_1\rangle)^2] + 1\,. \tag{9.19}$$

The variance in the quadratures is plotted in Fig. 9.2a versus the scaled driving field λ. The variance in the phase quadrature X_2 reaches a minimum at threshold. This minimum approaches $\frac{1}{2}$ as the threshold intensity is increased [10]. The value of one half in the variance of the intracavity field corresponds to zero fluctuations found at the resonance frequency in the external field. The fluctuations in the amplitude quadrature X_1 increase dramatically as the threshold is approached. However, unlike the calculation where the pump is treated classically the fluctuations do not diverge. This is because (9.17) is an exact solution to the nonlinear interaction including pump depletion. As the threshold value increases and therefore the number of pump photons required to reach threshold increases, the fluctuations become larger. In the limit $\gamma_1\gamma_2/\kappa^2 \to \infty$ the fluctuations diverge, as this corresponds to the classical pump (infinite energy). The variance in the amplitude quadrature above threshold continues to increase as the distribution is then double-peaked at the two stable output amplitudes.

The above solution demonstrates the usefulness of the complex *P* representation. Although the solution obtained for the steady state distribution has no interpretation in terms of a probability distribution, the moments calculated by integrating the distribution on a suitable manifold correspond to the physical moments. We have demonstrated how exact moments of a quantized intracavity field undergoing a nonlinear interaction may be calculated. To calculate the moments of the external field however, we must resort to linearization techniques.

9.2 Optical Parametric Oscillator: Positive *P* Function

As an alternative to the foregoing description we may consider the use of the positive *P* representation, following the treatment of *Wolinsky* and *Carmichael* [2]. We can obtain an analytic solution for the steady state positive *P* function. This solution is a

function of two phase space variables; one variable is the *classical field* amplitude, the other is a *non-classical variable* needed to represent superpositions of coherent states. A three-dimensional plot of the positive P function allows one to distinguish between the limiting regions of essentially classical behaviour and predominantly quantum behaviour.

We begin with the Langevin equations for the low frequency mode

$$\frac{\mathrm{d}\alpha}{\mathrm{d}\tau} = -\alpha - \beta(\lambda - \alpha^2) + g(\lambda - \alpha^2)^{1/2}\eta_1 \,, \tag{9.20}$$

$$\frac{\mathrm{d}\beta}{\mathrm{d}\tau} = -\beta - \alpha(\lambda - \beta^2) + g(\lambda - \beta^2)^{1/2}\eta_2 \,, \tag{9.21}$$

where τ is measured in cavity lifetimes (γ_1^{-1}),

$$g = \frac{\kappa}{(2\gamma_1\gamma_2)^{1/2}} \equiv \frac{1}{\mu} \,, \tag{9.22}$$

and λ is a dimensionless measure of the pump field amplitude scaled to give the threshold condition $\lambda = 1$, and we have scaled the c-number variables by

$$\alpha = g\alpha_1 \,, \qquad \beta = g\beta_1 \,. \tag{9.23}$$

Equations (9.20 and 9.21) describe trajectories in a four-dimensional phase space. The region of phase space satisfying the conjugacy condition $\beta = \alpha^*$ is called the *classical subspace*. Two extra non-classical dimensions are required by the quantum noise. If we neglect the fluctuating forces η_1 and η_2 (9.20 and 9.21) have the stable steady state solution $\alpha = \beta = 0$ below threshold $(\lambda < 1)$, and $\alpha = \beta = \pm(\lambda - 1)^{1/2}$ above threshold $(\lambda > 1)$. In the full phase space there are additional steady states which do not satisfy the conjugacy condition: two steady states $\alpha = \beta = \pm\mathrm{i}(1 - \lambda)^{1/2}$ below threshold and two steady states $\alpha = -\beta = \pm(\lambda + 1)^{1/2}$ both below and above threshold.

The variables α and β are restricted to a bounded manifold $\alpha = x,\ \beta = y$ with x and y both real and $|x|,\ |y| \leq \sqrt{\lambda}$. We denote this manifold by $\Lambda(x,\ y)$. Trajectories are confined within this manifold by reflecting boundary conditions. If a trajectory starts within this manifold, then it is clear from (9.20 and 9.21) that the drift and noise terms remain real, so a trajectory will remain on the real plane. Furthermore, at the boundary, the trajectory must follow the deterministic flow inwards, as the transverse noise component vanishes. If the initial quantum state is the vacuum state, the entire subsequent evolution will be confined to this manifold.

The manifold $\Lambda(x,\ y)$ is alternatively denoted by $\Lambda(u,\ \upsilon)$ with $u = \frac{1}{2}(x+y),\ \upsilon = \frac{1}{2}(x-y)$. The line $\upsilon = 0$ is a one-dimensional classical subspace, the subspace preserving $\alpha = \beta$. The variable υ denotes a transverse, non-classical dimension used by the noise to construct manifestly non-classical states.

We may now construct a pictorial representation of these states which dramatically distinguishes between the quantum and classical regimes.

With $\alpha = x,\ \beta = y$ both real, the solution to the Fokker-Planck equation (9.13) is of the form given by (9.17). With $|x|,\ |y| \leq \sqrt{\lambda}$

$$P_{\rm ss}(x,\ y) = N[(\lambda - x^2)(\lambda - y^2)]^{1/g^2 - 1} {\rm e}^{2xy/g^2}\ . \tag{9.24}$$

For weak noise $(g \ll 1)$, $P_{\rm ss}(x,\ y)$ is illustrated in Fig. 9.3. Below threshold $(\lambda < 1)$ $P_{\rm ss}(u,\ \upsilon)$ may be written

$$P_{\rm ss}(u,\ \upsilon) = \frac{(1-\lambda^2)^{1/2}}{\pi\lambda g/2} \exp\left(\frac{-(1-\lambda)u^2 + (1+\lambda)\upsilon^2}{\frac{\lambda g^2}{2}}\right)\ . \tag{9.25}$$

The normally-ordered field quadrature variances are determined by the quantities

$$\langle : \Delta X_1^2 : \rangle = V\left(\frac{\alpha+\beta}{2}\right)\ , \tag{9.26}$$

$$\langle : \Delta X_2^2 : \rangle = V\left(\frac{\alpha-\beta}{2}\right) \tag{9.27}$$

where $V(z)$ refers to the variance over the stationary distribution function. As $u = (\alpha+\beta)/2$ and $\upsilon = {\rm i}(\alpha-\beta)/2$, on the manifold $\Lambda(u,\ \upsilon)$, the quadrature variances are given by

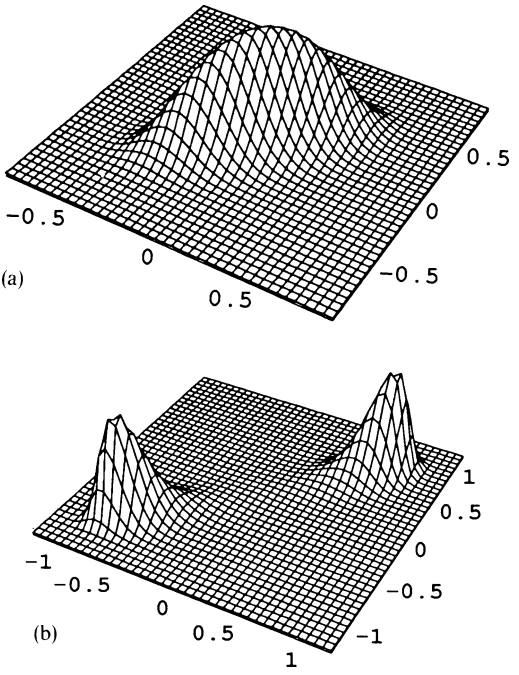

Fig. 9.3 A plot of the positive *P* representation of the steady state of the degenerate parametric amplifier, below and above threshold: (**a**) $\lambda = 0.8$ (**b**) $\lambda = 1.5$. In both cases $g = (2\varepsilon_2^{\rm c}/\kappa)^{-1/2} = 0.25$

$$\langle : \Delta X_1^2 : \rangle = V(u)/g^2 \,, \tag{9.28}$$

$$\langle : \Delta X_2^2 : \rangle = -V(\upsilon)/g^2 \,. \tag{9.29}$$

The variances $g^{-2}\langle \Delta u^2 \rangle$ and $-g^{-2}\langle \Delta \upsilon^2 \rangle$ correspond to the normally ordered variances of the unsqueezed and squeezed quadratures, respectively, of the subharmonic field.

The threshold distribution ($g \ll 1,\ \lambda = 1$) is given by

$$P_{\rm ss}(u,\ \upsilon) = \left[4\sqrt{\pi} g^{3/2} \Gamma\left(\frac{1}{4}\right)\right] {\rm e}^{-(u^4+4\upsilon^2)/g^2} \,. \tag{9.30}$$

Above threshold the distribution splits into two peaks. We note that in the low-noise regime $P_{\rm ss}(x,\ y)$ is a slightly broadened version of the classical steady state with only a small excursion into the nonclassical space.

Figure 9.4 shows $P_{\rm ss}(x,\ y)$ for the same values of λ as Fig. 9.3 but for the noise strength $g = 1$. The quantum noise has become sufficiently strong to explore

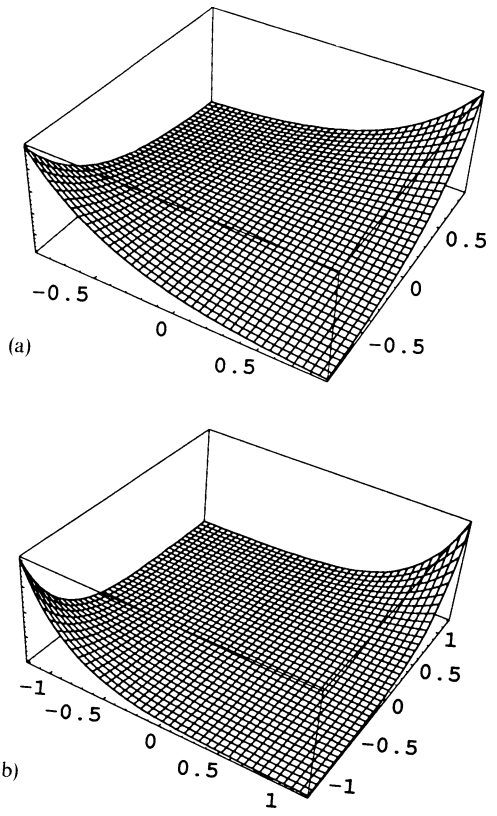

Fig. 9.4 As in Fig. 9.3 but with quantum noise parameter $g = 1.0$. (**a**) $\lambda = 0.8$ (**b**) $\lambda = 1.5$

thoroughly the non-classical dimension of the phase space. $P_{\rm ss}(x,\ y)$ is strongly influenced by the boundary $\Lambda(x,\ y)$.

As the noise strength g is increased beyond 1, the characteristic threshold behaviour of the parametric oscillator disappears and squeezing is significantly reduced (Fig. 9.5). In the large-g limit the stochastic trajectories are all driven to the boundary of $\Lambda(x,\ y)$, and then along this boundary to the corners, where both noise terms in (9.20 and 9.21) vanish. $P_{\rm ss}(x,\ y)$ approaches a sum of δ functions

$$\begin{aligned} P_{\rm ss}(x,y) =& \frac{1}{2}(1+\mathrm{e}^{4\lambda/g^2})^{-1}[\delta(x-\sqrt{\lambda})\delta(y-\sqrt{\lambda}) \\ &+\delta(x+\sqrt{\lambda})\delta(y+\sqrt{\lambda})] + \frac{1}{2}(1+\mathrm{e}^{4\lambda/g^2})^{-1} \\ &\times[\delta(x-\sqrt{\lambda})\delta(y+\sqrt{\lambda})+\delta(x+\sqrt{\lambda})\delta(y-\sqrt{\lambda})]\,. \end{aligned} \tag{9.31}$$

The two δ functions that set $x=-y=\pm\sqrt{\lambda}$ represent off-diagonal or interference terms $\mathrm{e}^{-2\sqrt{\lambda}/g}|\sqrt{\lambda}/g\rangle\langle-\sqrt{\lambda}/g|$. Figure 9.6a–c illustrates the behaviour of $P_{\rm ss}(x,\ y)$ as a function of λ in the strong-noise limit. When $4\lambda/g^2 \ll 1$ all δ functions carry equal weight and the state of the subharmonic field is the coherent state superposition $\frac{1}{2}(|\sqrt{\lambda}/g\rangle+|-\sqrt{\lambda}/g\rangle)$. As λ increases, this superposition state is replaced by a classical mixture of coherent states $|\sqrt{\lambda}/g\rangle$ and $|-\sqrt{\lambda}/g\rangle$ for $4\lambda/g^2 \gg 1$. This is a consequence of the competition between the creation of quantum coherence by the parametric process and the destruction of this coherence by dissipation. It will be shown in Chap. 15, that the decay of quantum coherence in a damped superposition state proceeds at a rate proportional to the phase space separation of the states.

This example has illustrated how quantum dissipative systems can exhibit manifestly quantum behaviour in the limit of large quantum noise. This is outside the realm of linear noise theory where classical states are only slightly perturbed.

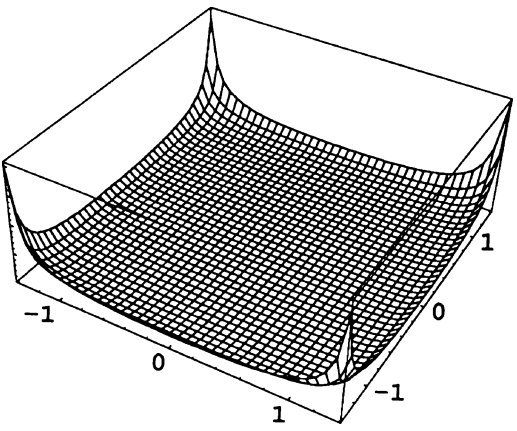

Fig. 9.5 As in Fig. 9.3 but with $\lambda = 1.5$ and $g = 10.0$

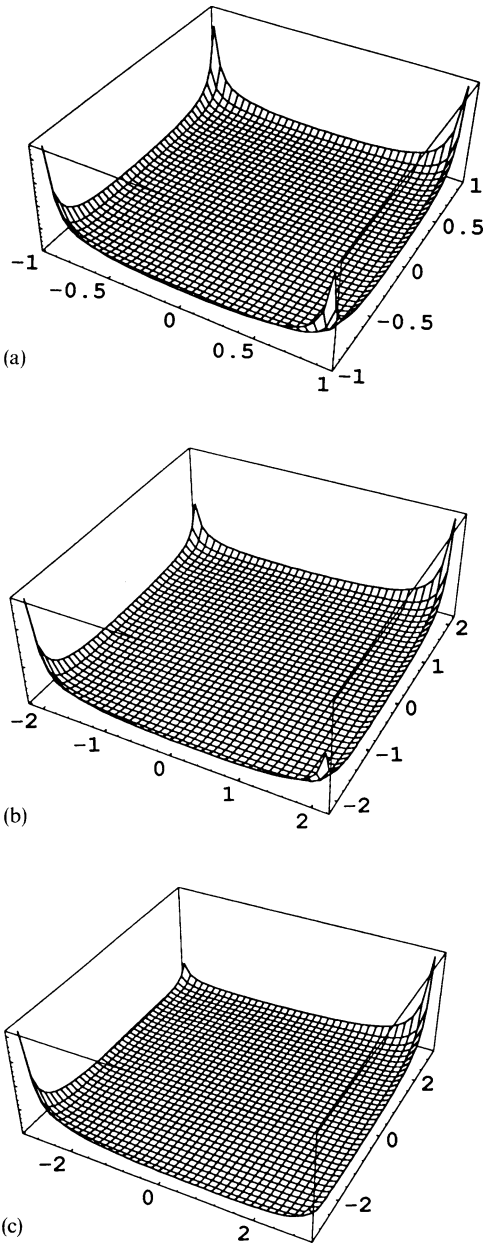

Fig. 9.6 As in Fig. 9.3 but demonstrating the dependence on λ with $g = 5.0$. (**a**) $\lambda = 1.0$ (**b**) $\lambda = 5.0$ (**c**) $\lambda = 10.0$

9.3 Quantum Tunnelling Time

We proceed to calculate the quantum tunnelling time between the two stable states. We shall follow the procedure of *Kinsler* and *Drummond* [3]. In order to calculate

the quantum tunnelling rate, we shall transform the variables α and β to give constant diffusion, or additive stochastic noise.

$$u = \sin^{-1}\left(\frac{g\alpha}{\sqrt{\lambda}}\right) + \sin^{-1}\left(\frac{g\beta}{\sqrt{\lambda}}\right) , \tag{9.32}$$

$$\upsilon = \sin^{-1}\left(\frac{g\alpha}{\sqrt{\lambda}}\right) - \sin^{-1}\left(\frac{g\beta}{\sqrt{\lambda}}\right) . \tag{9.33}$$

These new variables are constrained to have a range such that $|u| + |\upsilon| \leq \pi$. Referring back to the variables α and β, it can be seen that the u axis represents the classical subspace of the phase space where $\alpha = \beta$. Thus the variable υ is a non-classical dimension which allows for the creation of quantum features. The stochastic equations corresponding to these variables are

$$\mathrm{d}u = \left\{\lambda \sin(u) - \sigma\left[\tan\left(\frac{u+\upsilon}{2}\right) + \tan\left(\frac{u-\upsilon}{2}\right)\right]\right\}\mathrm{d}\tau + \sqrt{2}g\ \mathrm{d}W_u , \tag{9.34}$$

$$\mathrm{d}\upsilon = \left\{-\lambda \sin(\upsilon) - \sigma\left[\tan\left(\frac{u+\upsilon}{2}\right) - \tan\left(\frac{u-\upsilon}{2}\right)\right]\right\}\mathrm{d}\tau + \sqrt{2}g\ \mathrm{d}W_\upsilon . \tag{9.35}$$

Here $\sigma = 1 - g^2/2$, $\mathrm{d}W_u$, $\mathrm{d}W_\upsilon$ are Wiener processes.

These Ito equations have a corresponding Fokker–Planck equation and a probability distribution in the limit as $\tau \to \infty$ of

$$P(u,\ \upsilon) = N\ \exp[-V(u,\ \upsilon)/g^2] \tag{9.36}$$

where the potential $V(u,\ \upsilon)$ is

$$V(u,\ \upsilon) = -2\sigma \ln|\cos\ u + \cos\upsilon| + \lambda\cos\ u - \lambda\cos\upsilon . \tag{9.37}$$

Above threshold the potential has two minima corresponding to the stable states of the oscillator. These minima have equal intensities and amplitudes of opposite sign, and are at classical locations with $\alpha = \alpha^*$

$$(u_0,\ \upsilon_0) = (\pm 2\sin^{-1}[(\lambda - \sigma)^{1/2}/\sqrt{\lambda}], 0) \tag{9.38}$$

or

$$g\alpha_0 = \pm(\lambda - 1 + g^2)^{1/2} . \tag{9.39}$$

There is also a saddle point at $(u_s,\ \upsilon_s) = (0,\ 0)$.

Along the u axis the second derivative of the potential in the υ direction is always positive. The classical subspace $(\upsilon = 0)$ is therefore at a minimum of the potential with respect to variations in the non-classical variable υ. This valley along the u axis between the two potential wells is the most probable path for a stochastic trajectory in switching from one well to the other. The switching rate between them will be dominated by the rate due to trajectories along this route. Using an extension of Kramer's method, developed by *Landauer* and *Swanson* [4], the mean time taken for the oscillator to switch from one state to the other in the limit of $g^2 \ll 1$ is

$$T_p = \frac{\pi}{\gamma_1}\left(\frac{\lambda+\sigma}{\lambda(\lambda-\sigma)^2}\right)^{1/2} \exp\left\{\frac{2}{g^2}\left[\lambda-\sigma-\sigma\ln\left(\frac{\lambda}{\sigma}\right)\right]\right\} . \tag{9.40}$$

The switching time is increased as the pump amplitude λ is increased or the nonlinearity g^2 is reduced.

Previous attempts to compute the tunnelling time for this problem have used the Wigner function [5]. Unfortunately the time-evolution equation for the Wigner function contains third-order derivative terms and is thus not a Fokker–Planck equation. In the case of linear fluctuations around a steady state truncating the evolution equation at second-order derivatives is often a good approximation. However, it is not clear that this procedure will give quantum tunnelling times correctly.

In the limit of large damping in the fundamental mode the truncated Wigner function of the sub-harmonic mode obeys with $\tau = \gamma_1 t$

$$\frac{\mathrm{d}}{\mathrm{d}\tau}W(\beta,\,t) = \left\{\frac{\partial}{\partial\beta}[\beta-\beta^*(\lambda-g^2\beta^2)] + \frac{\partial}{\partial\beta^*}[\beta^*-\beta(\lambda-g^2\beta^{*2})] + \frac{\partial^2}{\partial\beta\partial\beta^*}(1+2g^2\beta\beta^*)\right\}W(\beta,\,\tau) . \tag{9.41}$$

This truncated Wigner function equation does not have potential solutions, however an approximate potential solution can be obtained that is valid near threshold. Here, the noise contribution $2g^2\beta\beta^*$ is small and is neglected leaving only subharmonic noise. Writing $\beta = x + \mathrm{i}p$, the solution in the near threshold approximation is

$$W_{\mathrm{NT}} = N_{\mathrm{NT}}\,\exp[-V_{\mathrm{NT}}(x,\,p)] \tag{9.42}$$

where

$$V_{\mathrm{NT}}(x,\,p) = \frac{2}{g^2}[g^2x^2+g^2p^2+\frac{1}{2}(g^2x^2+g^2p^2)^2-\lambda(g^2x^2-g^2p^2)] \tag{9.43}$$

and N_{NT} is the normalisation constant.

Above threshold this potential has two minima, at $gx = \pm(\lambda-1)^{1/2}$. In the limit of large-threshold photon numbers, these minima are very close to those obtained in (9.39). The tunneling time has been calculated from the Wigner distribution by *Graham* [6], with the result

$$T_{\mathrm{w}} = \frac{\pi}{\gamma_1}\left(\frac{\lambda+1}{\lambda(\lambda-1)^2}\right)^{1/2} \exp\left[\frac{1}{g}(\lambda-1)^2\right] . \tag{9.44}$$

This result is compared with the expression derived using the P function in Fig. 9.7 which shows the variation in the logarithm of the tunnelling rate with the pump amplitude λ. The Wigner function result predicts a slower switching time above threshold. The difference in the two predictions can be many orders of magnitude. The calculations from the exact positive P Fokker–Planck equation represent a true quantum tunnelling rate. Whereas the truncation of the Wigner function equation

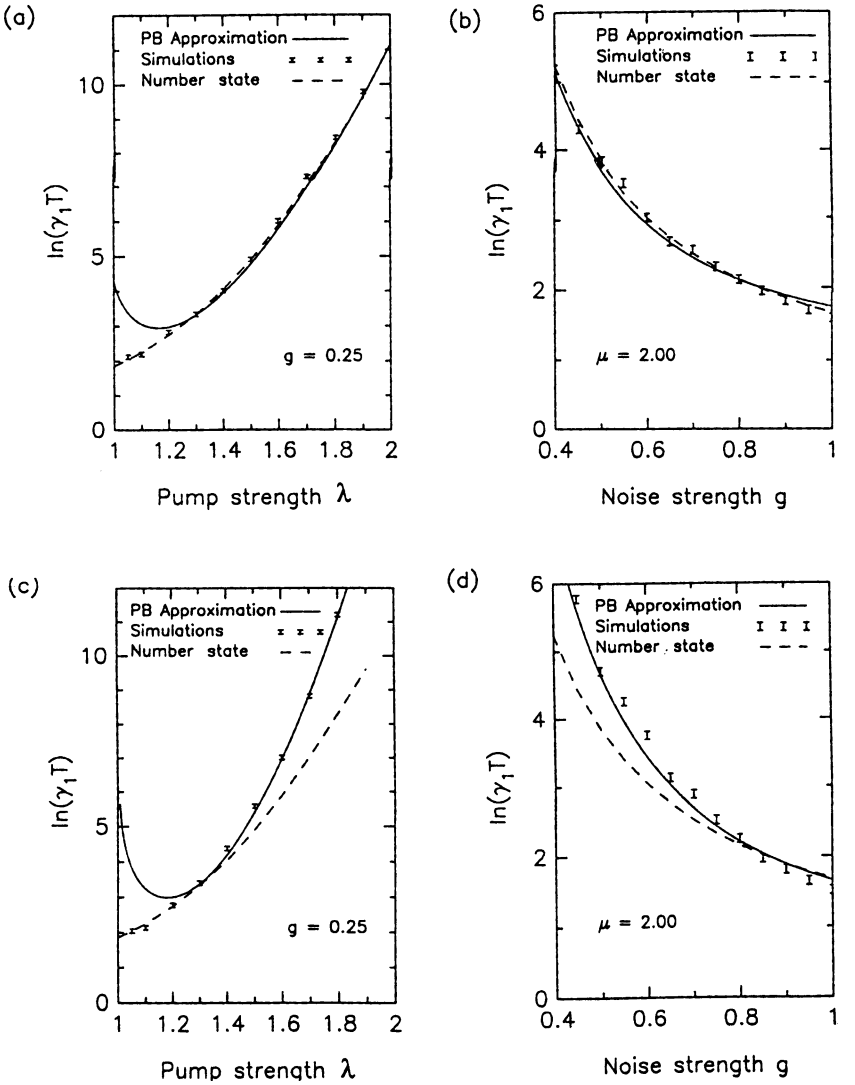

Fig. 9.7 A plot of the log of the tunnelling time for the degenerate parametric amplifier above threshold, versus pump strength or noise strength. In (**a**) and (**b**) we show the results computed by the positive *P* Representation (PB approximation) while in (**c**) and (**d**) we give the results for the truncated Wigner function model. In all cases we contrast the results obtained by potential methods with the results obtained by direct simulation of the corresponding stochastic differential equations and number state solution of the master equation (*dashed line*) [3]

involves dropping higher order derivatives dependent on the interaction strength g. Thus nonlinear terms in the quantum noise are neglected and the only quantum noise terms included are due to the vacuum fluctuations from the cavity losses. These give a diffusion term in the truncated Wigner Fokker–Planck equation which is identical

to classical thermal noise, with an occupation number of half a photon per mode. Also indicated in Fig. 9.7 are the tunnelling times computed by direct numerical simulation of the stochastic differential equations resulting from either the positive P representation (Fig. 9.7a, b) or the Wigner representation (Fig. 9.7c, d) and by directly solving the master equation in the number basis.

The differences between the two rates obtained reflect the difference between classical thermal activation and true quantum tunnelling. Classical thermal-activation rates are slower than quantum tunnelling rates far above threshold where the former are large since the thermal trajectory must go over the barrier. A quantum process, on the other hand, can short cut this by tunnelling.

9.4 Dispersive Optical Bistability

We consider a single mode model for dispersive optical bistability. An optical cavity is driven off resonance with a coherent field. The intracavity medium has an intensity dependent refractive index. As the intensity of the driving field is increased the cavity is tuned to resonance and becomes highly transmissive.

We shall model the intracavity medium as a Kerr type $\chi^{(3)}$ nonlinear susceptibility treated in the rotating wave approximation. The Hamiltonian is given by (5.79), The Fokker–Planck equation is

$$\frac{\partial P}{\partial t} = \left[\frac{\partial}{\partial \alpha}(\kappa\alpha + 2\mathrm{i}\chi\alpha^2\beta - E_0) - \mathrm{i}\chi\frac{\partial^2}{\partial\alpha^2}\alpha^2 \right.$$

$$\left. + \frac{\partial}{\partial\beta}(\kappa^*\beta - 2\mathrm{i}\chi\beta^2\alpha - E_0) + \mathrm{i}\chi\frac{\partial^2}{\partial\beta^2}\beta^2 \right] P(\alpha,\beta) \tag{9.45}$$

where we choose the phase of the driving field such that E_o is real and $\kappa = \gamma + \mathrm{i}\delta$. We shall seek a steady state solution using the potential conditions (6.72). The calculation of F gives

$$F_1 = -\left(\frac{i}{\chi}\right)\left(\frac{\bar{\kappa}}{\alpha} + 2\chi\beta - \frac{E_0}{\alpha^2}\right), \qquad F_2 = \left(\frac{i}{\chi^*}\right)\left(\frac{\bar{\kappa}^*}{\alpha} - 2\chi^*\beta - \frac{E_0}{\beta^2}\right), \tag{9.46}$$

where we have defined $\bar{\kappa} = \kappa - 2\mathrm{i}\chi$. The cross derivatives

$$\partial_\alpha F_2 = \partial_\beta F_1 = 2 \tag{9.47}$$

so that the potential conditions are satisfied.

The steady state distribution is given by

$$P_{\rm ss}(\alpha,\,\beta) = \exp\left[\int^{\alpha} F_\rho(\alpha')\mathrm{d}\alpha'_\rho\right]$$

$$= \exp\left\{\int^{\alpha}\left[\frac{1}{\mathrm{i}\chi}\left(\frac{\bar{\kappa}}{\alpha_1}+2\mathrm{i}\chi\beta_1-\frac{E_0}{\alpha_1^2}\right)\mathrm{d}\alpha_1-\frac{1}{\mathrm{i}\chi}\left(\frac{\bar{\kappa^*}}{\beta_1}-2\mathrm{i}\chi\alpha_1-\frac{E_0}{\beta_1^2}\right)\mathrm{d}\beta_1\right]\right\}$$

$$= \alpha^{c-2}\beta^{d-2}\exp\left[\left(\frac{E_0}{\mathrm{i}\chi}\right)\left(\frac{1}{\alpha}+\frac{1}{\beta}\right)+4\alpha\beta\right] \tag{9.48}$$

where $c = \frac{\kappa}{\mathrm{i}\chi}$, $d = \left(\frac{\kappa}{\mathrm{i}\chi}\right)^*$.

It can be seen immediately that the usual integration domain of the complex plane with $\alpha^* = \beta$ is not possible since the potential diverges for $\alpha\beta \to \infty$. However, the moments may be calculated using the complex P representation. The calculations are described in Appendix 9.A. The results for the mean amplitude $\langle a\rangle$ and correlation function $g^{(2)}(0)$ are plotted in Fig. 9.8 where they are compared with the semi-classical value for the amplitude $\alpha_{\rm SS}$.

It is seen that, whereas the semi-classical equation predicts a bistability or hysteresis, the exact steady state equation which includes quantum fluctuations does not exhibit bistability or hysteresis. The extent to which bistability is observed in practice will depend on the fluctuations, which in turn determine the time for random switching from one branch to the other. The driving field must be ramped in time intervals shorter than this random switching time in order for bistability to be observed.

The variance of the fluctuations as displayed by $g^{(2)}(0)$ show an increase as the fluctuations are enhanced near the transition point. The dip in the steady state mean at the transition point is due to out-of-phase fluctuations between the upper and lower branches.

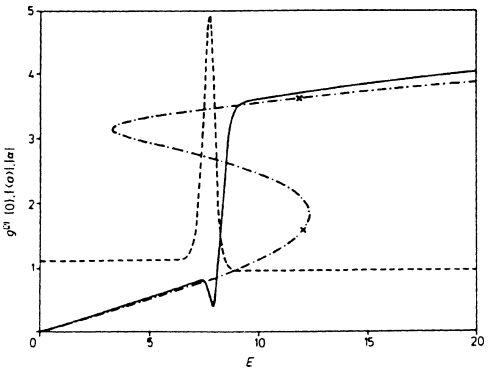

Fig. 9.8 The steady state amplitude, and second-order correlation function for optical bistability versus the pump amplitude. The chain curve gives the semi-classical steady state amplitude. The *full curve* gives the exact steady state amplitude. The *broken curve* presents the second-order correlation function $g^{(2)}(0)$. The detuning is chosen so that $\Delta\omega\chi < 0$ with $\Lambda\omega = -10$ and $\chi = 0.5$

9.5 Comment on the Use of the Q and Wigner Representations

We will compare the above solution we have obtained with the generalised P representation with the equation obtained using the Q and Wigner representations. With the Q representation we obtain the following equation

$$\frac{\partial Q}{\partial t}(\alpha^*,\alpha)=\left[\frac{\partial}{\partial\alpha}(-E_0+\bar{\kappa}\alpha+2i\chi\alpha^2\alpha^*)+i\chi\frac{\partial^2}{\partial\alpha^2}\alpha^2+(\kappa/2)\frac{\partial^2}{\partial\alpha\partial\alpha^*}+\text{c.c.}\right]Q(\alpha^*,\alpha) \tag{9.49}$$

where $\bar{\kappa}=\kappa-4i\chi+i\Delta\omega$.

This equation has a non-positive definite diffusion matrix. Furthermore, it does not satisfy the potential conditions, hence its steady-state solution is not readily obtained.

The equation for the Wigner function may be shown to be as in,

$$\begin{aligned}\frac{\partial W(\alpha^*,\alpha)}{\partial t}=\Bigg(&E_0\frac{\partial}{\partial\alpha}+\kappa\frac{\partial}{\partial\alpha}+\frac{\kappa}{2}\frac{\partial^2}{\partial\alpha^*\partial\alpha}-2i\chi\frac{\partial}{\partial\alpha}-i\chi\frac{1}{2}\frac{\partial^2}{\partial\alpha^{*2}}\alpha\\&+2i\chi\frac{\partial^3}{\partial\alpha^3}\alpha^*\alpha^2+\text{c.c.}\Bigg)W(\alpha^*,\alpha)\,.\end{aligned} \tag{9.50}$$

This equation is not of a Fokker–Planck form since it contains third-order derivatives. Again a steady-state solution is not readily obtainable. It is clear that for this problem the use of the complex P representation is preferable to the other two representations.

Exercises

9.1 Derive the Fokker–Planck equation for $P(\alpha_1,\ \alpha_2,\ t)$ for the non-degenerate parametric oscillation after adiabatically eliminating the pump mode. Solve for the potential solution and derive the moments.

9.2 Derive the evolution equations for the Q and Wigner functions for the degenerate parametric oscillator described by (9.1).

9.3 Derive the equation of motion for the Q function for optical bistability. Show that with zero detuning and zero driving the solution for an initial coherent state is

$$\begin{aligned}Q(\alpha,\ t)=&\exp(-|\alpha|^2)\sum_{q,\ p=0}^{\infty}(q!p!)^{-1}(\alpha\alpha_0^*)^q(\alpha^*\alpha_0)^p f(t)^{(p+q)/2}\\&\times\exp\left\{-|\alpha_0|^2\frac{[f(t)+i\delta]}{(1+i\delta)}\right\}\end{aligned}$$

where

$$\delta=(p-q)/\kappa\,,\qquad f(t)=\exp[-\kappa\nu-i\nu(p-q)]\,,\qquad \nu=2\mu t\,,\qquad \kappa=\frac{\gamma}{2\mu}\,.$$

9.4 Calculate the steady state distribution $P(\alpha)$ and the mean intensity $\langle \alpha^* \alpha \rangle$ for the degenerate parametric oscillator for the case where the thermal fluctuations dominate the quantum fluctuations.

9.A Appendix

9.A.1 Evaluation of Moments for the Complex P *function for Parametric Oscillation (9.17)*

It is necessary to integrate on a suitable manifold, chosen so that the distribution (9.17) and all its derivatives vanish at the boundary of integration. If we expand the term $\exp(2\alpha_1\ \beta_1)$ in (9.17) in a power series, the expression for the moment

$$I_{nn'} = \int\int \beta^n \alpha^{n'} P(\alpha) \mathrm{d}\alpha\ \mathrm{d}\beta\ . \tag{9.A.1}$$

can be written as

$$\begin{aligned} I_{nn'} = N(2|c|)^{2(j_2-2)} \sum_{m=0}^{\infty} \frac{2^{m+2}}{m!} \left(\frac{-c}{\kappa}\right)^{m+n-1} \left(\frac{-c^*}{\kappa}\right)^{m+n'+1} \\ \times \int\int z_1{}^{j_1-1}(1-z_1)^{j_2-j_1-1}(1-2z_1)^{m+n}(1-2z_2)^{m+n'} \\ \times z_2^{j_1-1}(1-z_2)^{j_2} \mathrm{d}z_1 \mathrm{d}z_2 \end{aligned} \tag{9.A.2}$$

where

$$j_1 = \frac{2\gamma_1\gamma_2}{\kappa^2}\ , \qquad j_2 = \frac{4\gamma_1\gamma_2}{\kappa^2}\ , \qquad z_1 = \frac{1}{2}\left(1+\frac{\kappa\alpha_1}{c}\right)\ , \qquad z_2 = \frac{1}{2}\left(1+\frac{\kappa\beta_2}{c^*}\right)\ .$$

These integrals are identical to those defining the Gauss' hypergeometric functions. The integration path encircles each pole and traverses the Riemann sheets so that the initial and final values of the integrand are equal, allowing partial integration operations to be defined. The result is [7].

$$\begin{aligned} I_{nn'} = N' \sum_{m=0}^{\infty} \frac{2^m}{m!} \left(\frac{-c}{\kappa}\right)^{m+n} \left(\frac{-c^*}{\kappa}\right)^{m+n'} \\ \times {}_2F_1(-(m+n), j_1, j_2, 2)\,{}_2F_1(-(m+n), j_1, j_2, 2) \end{aligned} \tag{9.A.3}$$

where ${}_2F_1$ are hypergeometric functions.

9.A.2 Evaluation of the Moments for the Complex P Function for Optical Bistability (9.48)

The normalization integral is

$$I(c,\,d)=\int_c\int\sum\frac{2^n}{n!}x^{-c-n}y^{-d-n}\exp\left[\frac{E_0}{\chi}(x+y)\right]\mathrm{d}x\,\mathrm{d}y \tag{9.A.4}$$

where we have made the variable change $x=1/\alpha$, $y=1/\beta$, and C is the integration path. $\alpha^*=\beta$ since the potential diverges for $|\alpha|^2\to\infty$. This means no Glauber–Sudarshan P function exists in the steady state (except as a generalised function). Hence, we shall use the complex P function where the paths of integration for α and β are line integrals on the individual $(\alpha,\,\beta)$ complex planes.

The integrand is now in a recognisable form as corresponding to a sum of gamma function integrals. It is therefore appropriate to define each path of integration to be a Hankel path of integration, from $(-\infty)$ on the real axis around the origin in an anticlockwise direction and back to $(-\infty)$. With this definition of the integration domain, the following gamma function identity holds [8]:

$$[\Gamma(c+n)]^{-1}=\left(\frac{t^{1-c-n}}{2\pi\mathrm{i}}\right)\int_c x^{-c-n}\exp(xt)\mathrm{d}x\,. \tag{9.A.5}$$

Hence, applying this result to both x and y integrations, one obtains with $\tilde{\chi}=\mathrm{i}\chi$

$$I(c,\,d)=-4\pi^2\sum_{n=0}^{\infty}\frac{2^n(E_0/\tilde{\chi})^{c+d+2(n-1)}}{n!\Gamma(c+n)\Gamma(d+n)}\,. \tag{9.A.6}$$

The series is a transcendental function which can be written in terms of the generalised Gauss hypergeometric series. That is, there is a hypergeometric series called ${}_0F_2$ which is defined as [9]

$${}_0F_2(c,\,d,\,z)=\sum_{n=0}^{\infty}\frac{z^n\Gamma(c)\Gamma(d)}{\Gamma(c+n)\Gamma(d+n)n!}\,. \tag{9.A.7}$$

From now on, for simplicity, we will write just $F()$, instead of ${}_0F_2()$. Now the normalisation integral can therefore be rewritten in the form

$$I(c,\,d)=\left(\frac{-4\pi^2|E_0/\tilde{\chi}|^{c+d-2}}{\Gamma(c)\Gamma(d)}\right)F(c,\,d,\,2|E_0/\tilde{\chi}|^2)\,. \tag{9.A.8}$$

The moments of the distribution function divided by the normalisation factor give all the observable one-time correlation functions. Luckily the moments have exactly the same function form as the normalisation factor [with the replacement of (c,d) by $(c+i,\,d+j)$] so that no new integrals need to be calculated. The ith-order correlation function is

$$G^{(i)} = \langle (a^\dagger)^i (a)^i \rangle = \left(\frac{|E_0/\tilde{\chi}|^{2i} \Gamma(c)\Gamma(d) F(i+c,\, i+d,\, 2|E_0/\tilde{\chi}|^2)}{\Gamma(i+c)\Gamma(i+d) F(c,\, d, 2|E_0/\tilde{\chi}|^2)} \right) . \quad (9.A.9)$$

This is the general expression for the ith-order correlation function of a nonlinear dispersive cavity with a coherent driving field and zero-temperature heat baths.

The results for the mean amplitude $\langle a \rangle$ and correlation function $g^2(0)$ are

$$\langle a \rangle = \frac{1}{c} \frac{|E_0/\tilde{\chi}| F(1+c,\, d,\, 2|E_0/\tilde{\chi}|^2)}{F(c,\, d,\, 2|E_0/\tilde{\chi}|^2)} , \quad (9.A.10)$$

$$g^{(2)}(0) = \left(\frac{cdF(c,\, d,\, 2|E_0/\tilde{\chi}|^2) F(c+2,\, d+2,\, 2|E_0/\tilde{\chi}|^2)}{(c+1)(d+1)[F(c+1,\, d+1,\, 2|E_0/\tilde{\chi}|^2)]^2} \right) . \quad (9.A.11)$$

References

1. P.D. Drummond, K.J. McNeil, D.F. Walls: Optica Acta **28**, 211 (1981)
2. M. Wolinsky, H.J. Carmichael: Phys. Rev. Lett. **60**, 1836 (1988)
3. P. Kinsler, P.D. Drummond: Phys. Rev. A **43**, 6194 (1991)
4. R. Landauer, S. Swanson: Phys. Rev. **121**, 1668 (1961)
5. P.D. Drummond, D.F. Walls: J. Phys. A**13** 725 (1980)
6. R. Graham: *Quantum Statistics in Optics and Solid State Physics*, Springer Tracts Mod. Phy., Vol. 66 (Springer, Berlin, Heidelberg 1973)
7. T.M. MacRobert: *Function of a Complex Variable* (Macmillan, London 1938)
8. M. Abramowitz, I.A. Stegun: *Handbook of Mathematical Function* (Dover, New York 1965)
9. I.S. Gradsteyn, I.M. Ryzhik: *Tables of Series, Products and Integrals*, (Deutsch, Frankfurt/M 1981)
10. G.J. Milburn, D.F. Walls: Optics Commun. **39**, 401 (1981)

Further Reading

Gibbs, H.: *Optical Bistability*, Academic Press (1985)
Lugiato, L.A. in *Progress in Optics*, p. 69, Ed. E. Wolf, North-Holland (1984)